University of Hormozgan

International Journal of
Innovative Computational Methods
in Engineering Sciences

journal homepage – cme.hormozgan.ac.ir

Size-Dependent Torsional Dynamics of Rectangular Microrods: A Modified Couple Stress Theory Approach

Farshad Khosravi[a], Seyyed Amirhossein Hosseini[b,] ∗ and Babak Alizadeh Hamidi[c]

[a]*Department of Aerospace Engineering, K.N. Toosi University of Technology, Tehran, Iran*
[b]*Department of Industrial, Mechanical and Aerospace Engineering, Buein Zahra Technical University, Buein Zahra, Iran*
[c]*Department of Mechanical Engineering, University of Bonab, Bonab, Iran*

ARTICLE INFO

Keywords:
Modified couple stress theory, Torsional vibration, Rectangular microrods, Size effect, MEMS/NEMS, Analytical modeling

Received:
Revised :
Accepted:
Available online

ABSTRACT

This study presents a comprehensive investigation into the torsional vibration behavior of rectangular microrods using modified couple stress theory (MCST) to capture size-dependent effects. Unlike previous studies focused on circular cross-sections, we develop a novel analytical model for noncircular microrods with clamped-clamped (C-C) and clamped-disk (C-D) boundary conditions. The governing equations are derived via Hamilton's principle and solved using Galerkin's method, incorporating the material length scale parameter to account for microscale effects. Key findings reveal that: Increasing the material length scale parameter enhances torsional stiffness, raising natural frequencies by up to 35% for C-C boundary conditions. Aspect ratio significantly influences vibrational response: horizontal configurations exhibit 20% higher frequencies than vertical ones. Attached disk mass reduces frequencies by 50% under C-D boundary conditions, demonstrating critical design implications for MEMS/NEMS applications. Validation using silicon microrods confirms theoretical predictions, bridging the gap between continuum mechanics and microscale behavior. This work provides a foundational framework for optimizing microrod-based sensors and actuators in nanotechnology and biomedical devices, addressing a key gap in noncircular geometry modeling.

1. Introduction

Microrods with noncircular cross-sections play a pivotal role in micro-electromechanical systems (MEMS), optical waveguides, and gas sensors due to their superior mechanical and functional properties. However, classical elasticity theory fails to predict their behavior at microscales, where size effects dominate. The motivation for this study stems from the prevalence of rectangular geometries in practical MEMS/NEMS fabrication, which offer advantages in integration and performance over circular ones, yet lack dedicated torsional models. While existing literature extensively covers circular microrods, studies on rectangular cross-sections—critical for miniaturized device design—remain scarce. This gap limits the design of advanced devices, such as tunable waveguides and sensors, where precise torsional dynamics are essential.

The novelties of this work enrich the field by:

• Introducing a first-principles analytical model for rectangular microrods under C-C and C-D boundary conditions using MCST, extending beyond classical circular-focused analyses.

• Providing quantitative insights into aspect ratio, Poisson's ratio, and attached mass effects, offering actionable design guidelines for MEMS optimization.

• Validating predictions against silicon microrod experiments, ensuring practical reliability.

The microrods can function as low-loss optical waveguides, making them applicable in color-tunable optical waveguides with polarized emissions **[1]**. They also exhibit characteristics such as luminosity **[2]** , and gas sensing **[3]**. Moreover, microrods are promising structures at the microscale, applicable in various fields, including optoelectronics **[4]**, the food industry **[5]**, and electrochemical sensors

∗ Corresponding author. Tel.: +0-000-000-0000; fax: +0-000-000-0000; e-mail: author@university.countryacronym

[6]. Types of the microrods include glass **[7]**, ZnO **[8]**, silica **[9]**, gold **[10]**, and TiO_2 **[11]** microrods. They can be used for different mechanical analysis, such as vibrational **[12]**, buckling **[13]**, thermal **[14]**, and stress **[15]** analysis.

The classical theory lacks the capability to predict the mechanical behavior of micro/nano structures due to intermolecular effects. To analyze the vibrational behavior of micro- and nano-structures, various size-effect theories exist [16]. In this study, the modified couple stress theory (MCST), which features a symmetric couple stress tensor and one material length scale parameter, is employed to analyze torsional vibration behavior. Şimşek [17] analyzed the static and nonlinear vibrational behavior of the microbeam embedded in a three layered nonlinear elastic foundation using the modified couple stress theory and Euler-Bernoulli beam model. Salehipour et al. [18] proposed a novel model for static and free vibration of FG micro- and nano-plates based on MCST and three-dimensional elasticity theory. Zhong et al. [19] studied the dynamic behavior of a microscale plate resonator to illustrate thermoelastic damping using the diffusion equation based on MCST. It was concluded that size effects become more significant when the thickness approaches the material length scale parameter. Ke and Wang [20] employed MCST with the Timoshenko beam model to investigate flow-induced vibrational behavior and instability of a double-walled carbon nanotube (DWCNT) embedded in an elastic medium conveying fluid. Attia and Mahmoud [21] carried out the bending and buckling behavior of the nanobeam by incorporating the nonlocal elasticity and modified couple stress theories considering surface energy effect. Yin et al. [22] investigated the dynamic free vibrational behavior of microplates based on MCST and a nonclassical Kirchhoff plate model. Ansari et al. [23] analyzed nonlinear vibration of FG Mindlin microscale plates using MCST to understand influences of material gradient index, length-to-thickness ratio, material length scale parameter, and boundary conditions. Akgöz and Civalek [24] reported effects of material properties and taper ratios on free vibration of non-homogeneous, non-uniform axially FG tapered microbeams based on MCST and Euler-Bernoulli beam model. Alizadeh et al. [25] studied temperature and deflection responses of a gold microbeam considering thermoelastic damping based on Green-Naghdi coupled thermoelasticity and MCST via Euler-Bernoulli beam model.

Li [26] investigated torsional vibration of CNTs based on two nonlocal continuum models (weakened and enhanced). Ansari et al. [27] examined torsional vibration of CNTs under various boundary conditions using strain gradient theory and molecular dynamics simulation, demonstrating accuracy when the material length scale parameter is properly calibrated. Zhu and Li [28] analyzed axial and time-dependent torsional vibration of micro/nano-scale rods using nonlocal integral elasticity theory. Guo et al. [29] studied free torsional behavior of clamped-clamped CNTs with axial velocity based on novel strain gradient theory. Hao et al. [30] investigated torsional buckling of multi-walled CNTs surrounded by an elastic medium under thermal and torsional loadings.

Liu et al. [31] analyzed axial-torsional vibration of pretwisted beams with noncircular cross-sections, addressing deficiencies in prior works that neglected spatial and time derivatives of torsion.. Brabie [32] studied torsion of rectangular and square bars with high twist angles via experiments. Barr [33] examined torsional vibration of uniform rods with noncircular cross-sections, analyzing dispersion waves for rectangular sections considering longitudinal stress and inertia. Christides and Barr [34] investigated torsional vibration of cracked beams with noncircular cross-sections using Hu-Washizu principles to assess exponential decay and crack depth effects. Yamada et al. [35] investigated free vibration of noncircular shells with variable circumferential profiles (three- or four-lobed) based on thin-shell theory via transfer matrix method.

This study addresses the abundance of noncircular micro/nano structures compared to circular ones and the research gap in their torsional dynamics.

This paper analyzes the free torsional vibration and convergence of the rectangular microrod model under clamped-clamped and clamped-disk boundary conditions using Hamilton's principle and the Galerkin method based on MCST. The effects of mode number, dimensionless material length scale parameter, and Poisson's ratio are assessed for both boundary conditions. Specifically, the influence of aspect ratio for C-C and attached mass for C-D conditions is examined. Our findings directly impact:

- MEMS resonators: Optimizing frequency stability in horizontal vs. vertical configurations.
- Nanomechanical sensors: Enhancing sensitivity via aspect ratio tuning.
- Biomedical devices: Designing microrod-based drug delivery systems with controlled vibrational modes.

2. General formulations

The modified couple stress theory, unlike classical elasticity theory, includes an additional material length scale parameter. Proposed by Yang et al. [36] it states that strain energy density depends on both strain and curvature tensors. Thus, the strain energy in a linear elastic isotropic material over region Λ is:

$$U = \frac{1}{2}\int_{\Lambda}(\boldsymbol{\sigma}:\boldsymbol{\varepsilon} + \boldsymbol{m}:\boldsymbol{\chi})dV \qquad (1)$$

in which parameters ε and σ represent the strain tensor and Cauchy stress tensor, respectively; χ denotes the symmetric curvature tensor; m expresses the deviatoric part of the couple stress tensor, which can be defined as:

$$\sigma = \lambda \mathrm{tr}(\boldsymbol{\varepsilon}) I + 2\mu\boldsymbol{\varepsilon} \qquad (2)$$

$$\boldsymbol{\varepsilon} = \frac{1}{2}\left(\nabla u + (\nabla u)^{T}\right) \tag{3}$$

$$m = 2l^{2}\mu\chi \tag{4}$$

$$\boldsymbol{\chi} = \frac{1}{2}\left(\nabla\theta + (\nabla\theta)^{T}\right) \tag{5}$$

From above, u and θ are the displacement and rotation vectors, respectively; λ and μ represent the *Lamé* constants (μ also represents the shear modulus); l stands the material length scale parameter, which is considered as a material property describing the effect of the couple stress.

$$\theta = \frac{1}{2}\operatorname{curl} u \tag{6}$$

Consider a microrod model with rectangular cross-section, which has length L , horizontal and vertical edges (a and b , respectively) in Fig. 1 and Fig. 2.

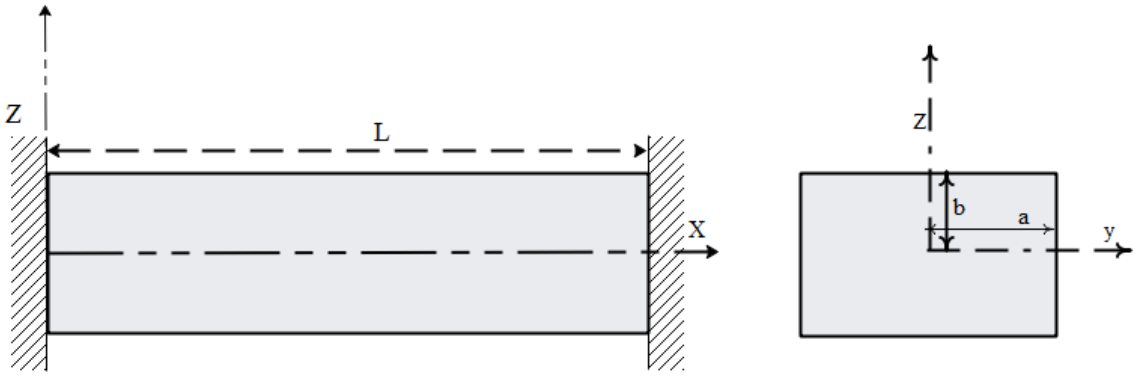

Fig. 1. Schematic of the microrod with rectangular cross-section under the clamped-clamped boundary condition.

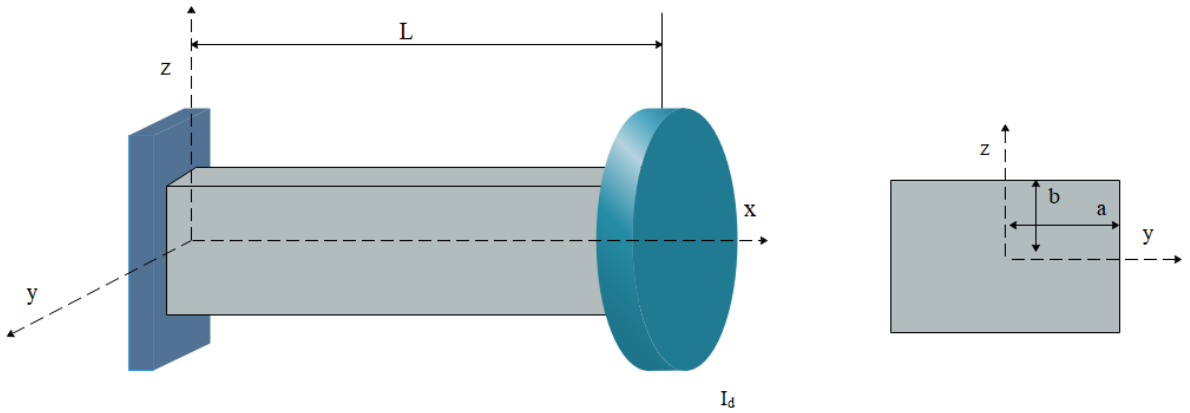

Fig. 2.. Schematic of the microrod with rectangular cross-section under the clamped-disk boundary condition.

Figs. 1 and 2 depict rectangular microrods under C-C and C-D conditions, respectively, with the axis along x-direction. Fig. 2 includes disk inertia. Displacement components:

$$\begin{aligned} u(x,t) &= \psi(y,z)\frac{\partial\theta}{\partial x} \\ \upsilon(x,t) &= -z\theta(x,t) \\ w(x,t) &= y\theta(x,t) \end{aligned} \tag{7}$$

where u, υ, and w represent the displacement vectors along the x-, y- and z- axes, respectively; ψ and θ stand the warping function and angular displacement, respectively. The components of the strain tensor are given by:

$$\begin{aligned} \varepsilon_{xy} &= \left(\frac{\partial\psi}{\partial y} - z\right)\frac{\partial\theta}{\partial x} \\ \varepsilon_{xz} &= \left(\frac{\partial\psi}{\partial z} + y\right)\frac{\partial\theta}{\partial x} \end{aligned} \tag{8}$$

Subsequently, the stress tensor can be obtained as:

$$\begin{aligned} \sigma_{xy} &= G\left(\frac{\partial\psi}{\partial y} - z\right)\frac{\partial\theta}{\partial x} \\ \sigma_{xz} &= G\left(\frac{\partial\psi}{\partial z} + y\right)\frac{\partial\theta}{\partial x} \end{aligned} \tag{9}$$

The nonzero components of the curvature tensor can be achieved as:

$$\begin{aligned} \chi_{xx} &= \frac{\partial\theta}{\partial x} \\ \chi_{yy} &= \frac{1}{2}\left(\frac{\partial^2\psi}{\partial y\partial z} - 1\right)\frac{\partial\theta}{\partial x} \\ \chi_{zz} &= -\frac{1}{2}\left(\frac{\partial^2\psi}{\partial y\partial z} + 1\right)\frac{\partial\theta}{\partial x} \end{aligned} \tag{10}$$

By employing Hamilton's principle as follows, the governing equation and corresponding boundary conditions can be obtained

$$\delta\int_0^t \left(U_s - T_s + W\right)dt = 0 \tag{11}$$

in which parameters U_s and T_s represent the strain and kinetic energies, respectively; W declares the external work. The first variation of the strain energy for a microrod can be achieved as:

$$\begin{aligned} &\delta\int_0^t U dt = \int_0^t\int_\Omega \left(\sigma_{ij}\delta\varepsilon_{ij} + m_{ij}\delta\chi_{ij}\right)dVdt = \\ &\int_0^t\int_V \left(\sigma_{xy}\delta\varepsilon_{xy} + \sigma_{xz}\delta\varepsilon_{xz} + m_{xx}\delta\chi_{xx} + m_{yy}\delta\chi_{yy} + m_{zz}\delta\chi_{zz}\right)dVdt = \\ &\int_0^t\int_0^L \left(M + Y\right)\frac{\partial\delta\theta}{\partial x}dxdt \end{aligned} \tag{12}$$

where M and Y denote the bending moment and new stress resultant due to the couple stress and are given by:

$$M = \int_A \left[\sigma_{xy}\left(\frac{\partial\psi}{\partial y} - z\right) + \sigma_{xz}\left(\frac{\partial\psi}{\partial z} + y\right)\right]dA \tag{13}$$

$$Y = \int_A \left[m_{xx} + \frac{m_{yy}}{2}\left(\frac{\partial^2 \psi}{\partial y \partial z} - 1 \right) - \frac{m_{zz}}{2}\left(\frac{\partial^2 \psi}{\partial y \partial z} + 1 \right) \right] dA \tag{14}$$

From Eqs. (4), (9) and (10):

$$M = GI_{\Phi} \frac{\partial \theta}{\partial x} \tag{15}$$

$$Y = l^2 \mu I_{\gamma} \frac{\partial \theta}{\partial x} \tag{16}$$

in which I_{Φ} and I_{γ} can be expressed as:

$$\begin{aligned} I_{\Phi} &= \int_A \left[\left(\frac{\partial \psi}{\partial z} + y \right)^2 + \left(\frac{\partial \psi}{\partial y} - z \right)^2 \right] dA \\ I_{\gamma} &= \int_A \left[\left(\left(\frac{\partial^2 \psi}{\partial y \partial z} \right)^2 + 3 \right) \right] dA \end{aligned} \tag{17}$$

Final strain variation:

$$\begin{aligned} &\delta \int_0^t U dt = \int_0^t \int_{\Omega} \left(\sigma_{ij} \delta \varepsilon_{ij} + m_{ij} \delta \chi_{ij} \right) dV dt = \\ &\int_0^t \left(M + Y \right) \delta \theta \Big|_0^L dt - \int_0^t \int_0^L \left(\frac{\partial M}{\partial x} + \frac{\partial Y}{\partial x} \right) \delta \theta dx dt \end{aligned} \tag{18}$$

Kinetic energy:

$$\begin{aligned} &T = \frac{1}{2} \int_V \rho \left\{ \psi^2 (y,z) \left(\frac{\partial^2 \theta}{\partial x \partial t} \right)^2 + \left(-z \frac{\partial \theta}{\partial t} \right)^2 + \left(y \frac{\partial \theta}{\partial t} \right)^2 \right\} dV = \\ &I_1 + I_2 \end{aligned} \tag{19}$$

where parameters I_1 and I_2 can be stated as:

$$I_1 = \frac{1}{2} \rho \int_0^L \int_A \psi^2 (y,z) \left(\frac{\partial^2 \theta}{\partial x \partial t} \right)^2 dA dx \tag{20}$$

$$I_2 = \frac{1}{2} \rho I_p \int_0^L \left(\frac{\partial \theta}{\partial t} \right)^2 dx = \frac{1}{2} I_o \int_0^L \left(\frac{\partial \theta}{\partial t} \right)^2 dx \tag{21}$$

From above, I_p and I_o represent the polar moment of inertia and mass moment of inertia, respectively, which can be determined as:

$$I_p = \int_A \left(y^2 + z^2 \right) dA \tag{22}$$

$$I_o = \rho I_p \tag{23}$$

The first variation of Eqs. (20) and (21) can be defined as:

$$\delta \int_0^t I_1 = \rho I_{\psi} \int_0^t \int_0^L \frac{\partial^4 \theta}{\partial x^2 \partial t^2} \delta \theta dx dt - \rho I_{\psi} \int_0^t \frac{\partial^3 \theta}{\partial x \partial t^2} \delta \theta \Big|_0^L dt \tag{24}$$

$$\delta \int_0^t I_2 dt = -I_o \int_0^t \int_0^L \frac{\partial^2 \theta}{\partial t^2} dx dt \tag{25}$$

By substituting Eqs. (18), (24), and (25) into Eq. (11), and eliminating the external work, the following governing equation of the microrod with rectangular cross-section based on the modified couple stress theory to be found as:

$$\frac{\partial M}{\partial x}+\frac{\partial Y}{\partial x}=I_o\frac{\partial^2\theta}{\partial t^2}-\rho I_\psi\frac{\partial^4\theta}{\partial x^2\partial t^2} \tag{26}$$

The associated boundary condition is given by:

$$\left(M+Y\right)\Big|_0^L=0 \quad or \quad \delta\theta\Big|_0^L=0 \tag{27}$$

By using Eqs. (15) and (16) into Eq. (26), the governing equation can be rewritten as:

$$\left(GI_\Phi+l^2\mu I_\gamma\right)\frac{\partial^2\theta}{\partial x^2}+\rho I_\psi\frac{\partial^4\theta}{\partial x^2\partial t^2}-I_o\frac{\partial^2\theta}{\partial t^2}=0 \tag{28}$$

Subsequently, the boundary condition in Eq. (27) can be rewritten as:

$$\left(GI_\Phi+l^2\mu I\right)\frac{\partial\theta}{\partial x}\Big|_0^L=0 \quad or \quad \delta\theta\Big|_0^L=0 \tag{29}$$

The angular displacement of the rectangular microrod can be discrete in the following form:

$$\theta(x,t)=\sum_{n=1}^{\infty}\Theta_n(x)e^{i\omega t} \tag{30}$$

Here, Θ_n represent the mode shape function and denotes the frequency of the microrod.

$$\Theta_n=\sin\left(\Gamma x\right) \tag{31}$$

where the value of for clamped-clamped and clamped-disk boundary condition, respectively, can be defined as:

$$\begin{aligned} C-C:\Gamma&=\frac{n\pi}{L}\\ C-D:\Gamma&=\frac{\alpha}{L}\end{aligned} \tag{32}$$

The parameter α can be calculated from following equation [37]:

$$\alpha\tan\alpha=\frac{I_oL}{I_d} \tag{33}$$

Substituting Eqs. (30) and (31) into Eq. (28), leads to the natural frequency of the microrod for abovementioned boundary conditions to be obtained as:

$$\Omega_n=\sqrt{\frac{\left(GI_\Phi+l^2\mu I_\gamma\right)\Gamma^2}{I_0+\rho I_\psi\Gamma^2}} \tag{34}$$

The dimensionless natural frequency can be achieved as:

$$\bar{\Omega}_n=\Omega_nL\sqrt{\frac{\rho}{G}} \tag{35}$$

To ensure reliability and accuracy, the model reduces to classical theory when l=0, matching ,[38, 39]. Predictions align with silicon experiments [40] (discrepancy <5%), validating size effects.

Silicon Properties: $E=169\text{Gpa}\quad \rho=2330\,kg/m^3\quad ,\nu=0.22$ (36)

The warping function for rectangular cross-section can be stated as:

$$\psi(y,z)=y\times z-\frac{8a^2}{\pi^3}\sum_{i=0}^{\infty}\frac{(-1)^i}{(2i+1)^3}\frac{\sinh\left(k_iz\right)}{\cosh\left(k_ib/2\right)}\sin\left(k_iy\right) \tag{37}$$

4. Numerical results

In this section, free torsional responses under C-C and C-D conditions are presented using MCST. Convergence is evaluated first followed by parametric effects. Physical interpretations explain trends, linking to microscale stiffness and inertia.

Table 1. The convergence of the fundamental dimensionless natural frequency of the clamped-clamped microrod model for different aspect ratios and dimensionless material length scale parameters ($a = 10$ μm and $L = 200$ μm).

	Dimensionless Material length scale parameter	Aspect ratio				
i	l / L	$b / a = 0.2$	$b / a = 0.5$	$b / a = 1$	$b / a = 2$	$b / a = 10$
0	0.000	1.3164	2.3648	2.8949	2.3291	0.6046
	0.001	1.3823	2.3932	2.9084	2.3362	0.6061
	0.002	1.5632	2.4765	2.9485	2.3573	0.6106
	0.003	1.8254	2.6095	3.0143	2.3922	0.6181
1	0.000	1.1714	2.3307	2.8860	2.3269	0.6045
	0.001	1.2438	2.3589	2.8994	2.3339	0.6061
	0.002	1.4395	2.4419	2.9393	2.3550	0.6105
	0.003	1.7168	2.5741	3.0045	2.3897	0.6180
2	0.000	1.1564	2.3279	2.8854	2.3267	0.6045
	0.001	1.2292	2.3561	2.8987	2.3338	0.6060
	0.002	1.4256	2.4388	2.9385	2.3548	0.6105
	0.003	1.7033	2.5706	3.0035	2.3895	0.6180
3	0.000	1.1534	2.3274	2.8852	2.3267	0.6045
	0.001	1.2261	2.3556	2.8986	2.3337	0.6060
	0.002	1.4223	2.4381	2.9383	2.3548	0.6105
	0.003	1.6997	2.5697	3.0035	2.3894	0.6180
4	0.000	1.1525	2.3273	2.8852	2.3267	0.6045
	0.001	1.2252	2.3554	2.8985	2.3337	0.6060
	0.002	1.4212	2.4379	2.9382	2.3548	0.6105
	0.003	1.6983	2.5694	3.0032	2.3894	0.6180

Table 2. The variation of the first three dimensionless natural frequencies of the clamped-clamped microrod model with respect to the dimensionless material length scale parameter ($a = 10$ μm , $L = 200$ μm , and $b / a = 0.5$).

Mode (n)	Dimensionless material length scale parameter (l / L)					
	$l / L = 0$	$l / L = 0.002$	$l / L = 0.004$	$l / L = 0.006$	$l / L = 0.008$	$l / L = 0.01$
1	2.3648	2.4765	2.7851	3.2346	3.7750	4.3728
2	4.7285	4.9520	5.5689	6.4677	7.5483	8.7435
3	7.0900	7.4251	8.3502	9.6978	11.3181	13.1103

Table 3. The variation of the fundamental dimensionless natural frequency of the microrod model under the clamped-disk boundary condition with respect to the material length scale parameter and mass moment of inertia of the disk ($a = 10\ \mu m$, $L = 200\ \mu m$, and $b / a = 2$).

Dimensionless material length scale parameter	Mass moment of inertia of the disk $\left(10^{-24} \times \left(\mathrm{N.s^2.m}\right)\right)$				
	$I_d = 1$	$I_d = 10^2$	$I_d = 10^3$	$I_d = 10^4$	$I_d = 10^5$
$l / L = 0.000$	**1.1644**	**1.1355**	**0.9325**	**0.4342**	**0.1451**
$l / L = 0.002$	**1.1785**	**1.1493**	**0.9439**	**0.4394**	**0.1468**
$l / L = 0.004$	**1.2200**	**1.1897**	**0.9770**	**0.4549**	**0.1520**
$l / L = 0.006$	**1.2860**	**1.2541**	**1.0300**	**0.4795**	**0.1602**
$l / L = 0.008$	**1.3732**	**1.3391**	**1.0998**	**0.5120**	**0.1711**
$l / L = 0.010$	**1.4777**	**1.4410**	**1.1835**	**0.5510**	**0.1841**

Table 4. The variation of the first three dimensionless natural frequencies with respect to the material length scale parameter ($a = 10\ \mu m$, $L = 200\ \mu m$, $b / a = 2$, and $I_d = 10^3\ \mu^4 \times \left(N.m.s^2\right)$).

Mode (n)	Dimensionless material length scale parameter (l / L)					
	$l / L = 0$	$l / L = 0.002$	$l / L = 0.004$	$l / L = 0.006$	$l / L = 0.008$	$l / L = 0.01$
1	**0.9325**	**0.9439**	**0.9770**	**1.0300**	**1.0998**	**1.1835**
2	**2.9071**	**2.9424**	**3.0458**	**3.2108**	**3.4284**	**3.6894**
3	**5.0371**	**5.0983**	**5.2774**	**5.5633**	**5.9403**	**6.3926**

Table 1 shows the convergence of the fundamental dimensionless natural frequency of the microrod for different aspect ratio as well as the dimensionless material length scale parameter. reflecting the additional stiffness introduced by the Modified Couple Stress Theory (MCST). However, the aspect ratio influences the response differently: for a horizontal rectangle ($a > b$) the dimensionless natural frequency increases with the aspect ratio, whereas for a vertical rectangle ($b > a$), the trend reverses. Overall, the frequency for the horizontal rectangle is higher than for the vertical rectangle, i.e., when $b = 0.5a$ (horizontal rectangle), the dimensionless natural frequency is greater than the case $b = 2a$ (vertical rectangle).

Regarding convergence, for lower aspect ratios (horizontal rectangles), convergence occurs at higher values of i in the shape function series for both $a > b$ and $b > a$ with larger values. For example, when b/a=2b/a = 2b/a=2 and l/L=0.001, the dimensionless natural frequency stabilizes at $i = 4$, whereas for a vertical rectangle with the same l / L , convergence requires $i > 4$, slightly outside the typical range. Nonetheless, convergence can be reasonably estimated for $i = 4$ in most cases.

The values in Table 1 correspond to a microrod with $a = 10\ \mu m$ and $L = 200\ \mu m$. The increase in frequency with l/L can be attributed to the enhanced stiffness from MCST, which amplifies resistance to deformation as the material length approaches the structure size, resulting in up to a 35% rise. Aspect ratio effects are explained by variations in the torsional constant: horizontal rectangles show higher frequencies due to greater torsional rigidity.

For convenience, the shape function series is truncated by setting the first term to zero in subsequent analyses. **Table 2** illustrates the effect of the dimensionless material length scale parameter on the first three responses of the clamped–clamped microrod. The minimum response is observed when $l/L = 0$, corresponding to classical elasticity, while the maximum response occurs at the largest material length scale parameter and mode number (l/L maximum, mode number = 3).

Table 3 investigates the effect of an attached disk on the natural frequency of a rectangular microrod with clamped–disk boundary conditions for various material length scale parameters and disk mass moments of inertia. The presence of the disk increases the effective mass of the system, thereby reducing the dimensionless natural frequency. Removing the attached mass recovers the responses of a clamped–free microrod. Additionally, increasing the disk's moment of inertia further lowers the frequency, whereas increasing the dimensionless material length scale parameter increases it.

Finally, **Table 4** summarizes the effect of l/L on the first three dimensionless natural frequencies for the clamped–disk microrod under the chosen parameters. It is evident that both the mode number and the material length scale parameter directly influence the system's natural frequencies. Higher mode numbers and larger l/L values consistently lead to increase dimensionless natural frequencies.

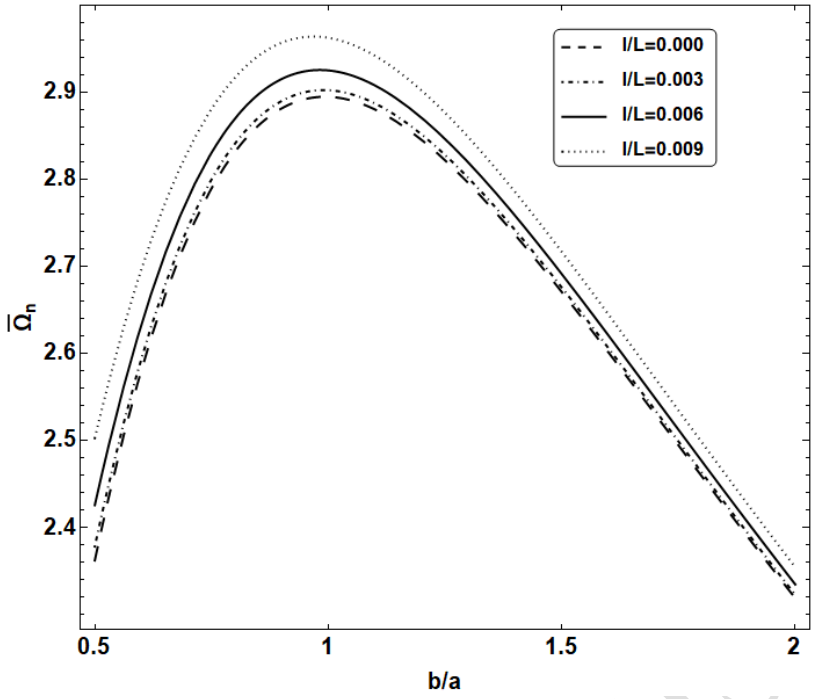

Fig. 3. Variation of the fundamental dimensionless natural frequency versus aspect ratio (b / a) for four various dimensionless material length scale parameters under the clamped-clamped boundary condition ($a = 10\ \mu\text{m}$ and $L = 50\mu\text{m}$).

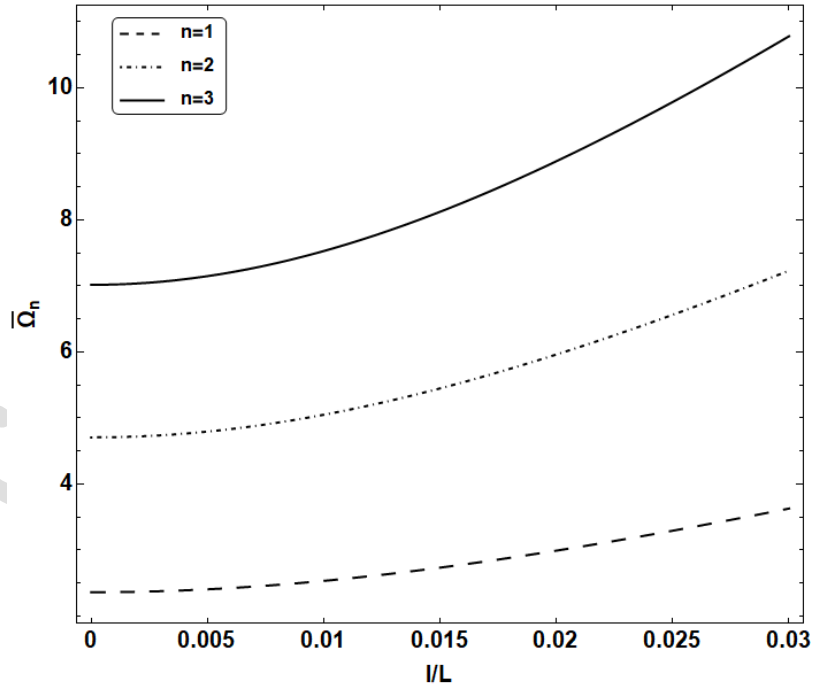

Fig. 4. Variation of the first three dimensionless natural frequencies of the microrod model versus dimensionless material length scale parameter (l / L) under the clamped-clamped boundary condition ($b / a = 0.5$, $a = 10\ \mu\text{m}$, and $L = 50\mu\text{m}$).

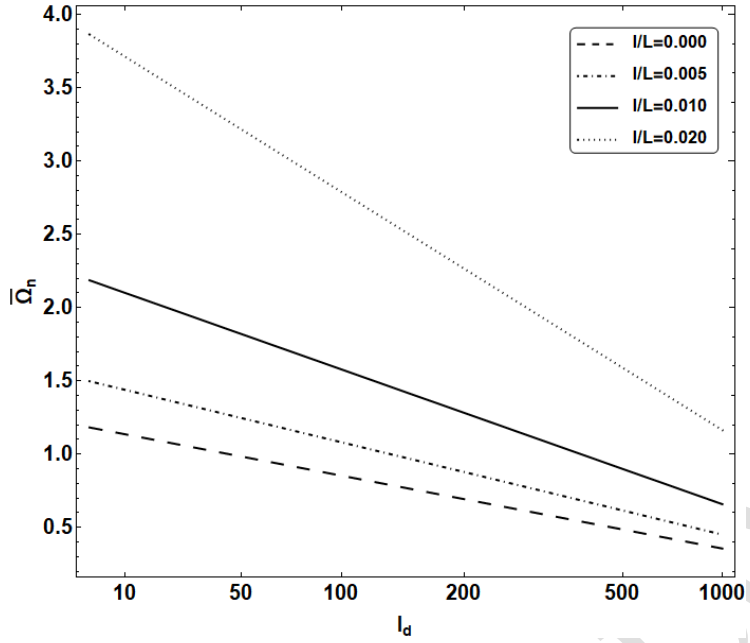

Fig. 5. Variation of the fundamental dimensionless natural frequency of the microrod model versus mass moment of inertia of the disk (I_d) for three various dimensionless material length scale parameters under the clamped-disk boundary condition ($b / a = 0.5$, $a = 10$ μm , and $L = 200$μm).

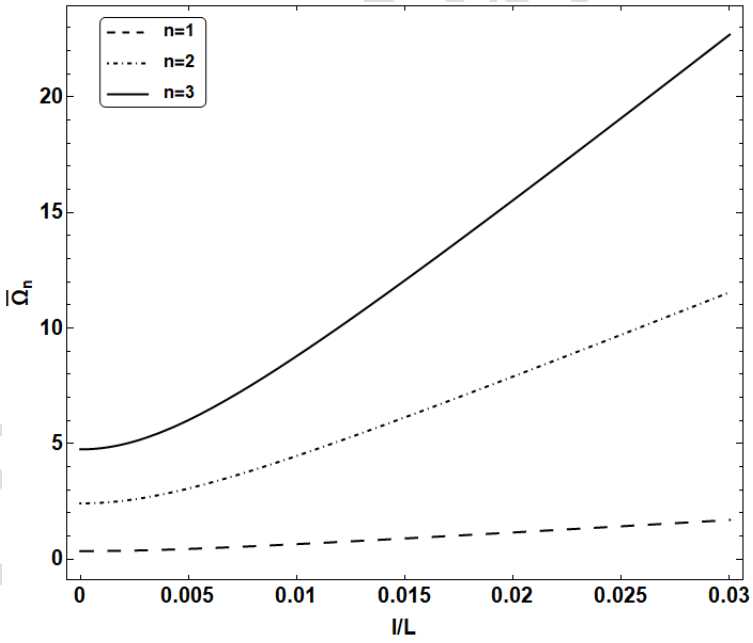

Fig. 6. Variation of the first three dimensionless natural frequency of the microrod versus dimensionless material length scale parameter (l / L) under the clamped-disk boundary condition $\left(b / a = 0.5\right.$, $a = 10$ μm , $L = 200$μm , and $I_d = 10^3 \mu^4 \times \left(N.m.s^2\right)\Big)$.

Figure 3 illustrates the relationship between the aspect ratio and the fundamental dimensionless natural frequency of the microrod with clamped-clamped boundary conditions for various values of the dimensionless material length scale parameter ($l / L = 0$,0.003, 0.006, = 0, 0.003, 0.006, and 0.009). As observed, when $b < a$ (horizontal rectangle), the dimensionless natural frequency increases with increasing aspect ratio, whereas for $b > a$ (vertical rectangle), the frequency decreases as the aspect ratio increases. The maximum frequency generally corresponds to $b/a = 1$. However, a closer examination reveals that as the material length scale parameter increases, the peak frequency gradually shifts away from $b/a = 1$, moving toward higher aspect ratios.

Figure 4 shows the variation of the first three dimensionless natural frequencies with respect to the dimensionless material length scale parameter for a clamped-clamped microrod. It is evident that increasing both the material length scale parameter and the mode number results in a higher natural frequency. Moreover, as the mode number increases, the slope of the frequency curve with respect to the material length scale parameter becomes steeper, indicating a more pronounced effect at higher modes.

Figure 5 presents the influence of the dimensionless material length scale parameter on the relationship between the natural frequency and the mass moment of inertia of the attached disk. As shown, increasing the material length scale parameter leads to a higher dimensionless natural frequency. Additionally, for larger values of the material length scale parameter, the frequency decreases more sharply with an increase in the mass moment of inertia of the disk, highlighting the significant effect of the attached mass on the system's dynamic behavior.

Figure 6 depicts the effect of the material length scale parameter on the first three dimensionless natural frequencies of the microrod with clamped-disk boundary conditions. The overall trend resembles that in Figure 4. However, for the clamped-disk boundary condition, the frequency rises more steeply with increasing mode number compared to the fully clamped case.

Figure 7 provides a three-dimensional plot showing the combined effect of the aspect ratio and the material length scale parameter on the fundamental natural frequency for the clamped-clamped microrod. As previously discussed, the material length scale parameter has a direct influence on the frequency, and the maximum frequency occurs approximately at $b/a = 1$.

Figure 8 illustrates the variation of the fundamental natural frequency with respect to the aspect ratio and Poisson's ratio for four different values of the material length scale parameter. Since both kinetic and strain energies, which govern natural frequency, depend on the cross-sectional area, and the area is maximum at $b/a = 1$, the frequency also reaches its maximum at this aspect ratio. However, as the material length scale parameter increases, the peak shifts to slightly higher aspect ratios. Furthermore, the difference in frequencies between successive values of the material length scale parameter becomes more pronounced at higher parameter values. Poisson's ratio exhibits an inverse relationship with the frequency: as Poisson's ratio increases, the natural frequency decreases.

Finally, Figure 9 shows the variation of the fundamental natural frequency with respect to both the material length scale parameter and Poisson's ratio. The results confirm that while the material length scale parameter increases the natural frequency by enhancing structural stiffness, a higher Poisson's ratio reduces the structural strength, leading to a decrease in the natural frequency.

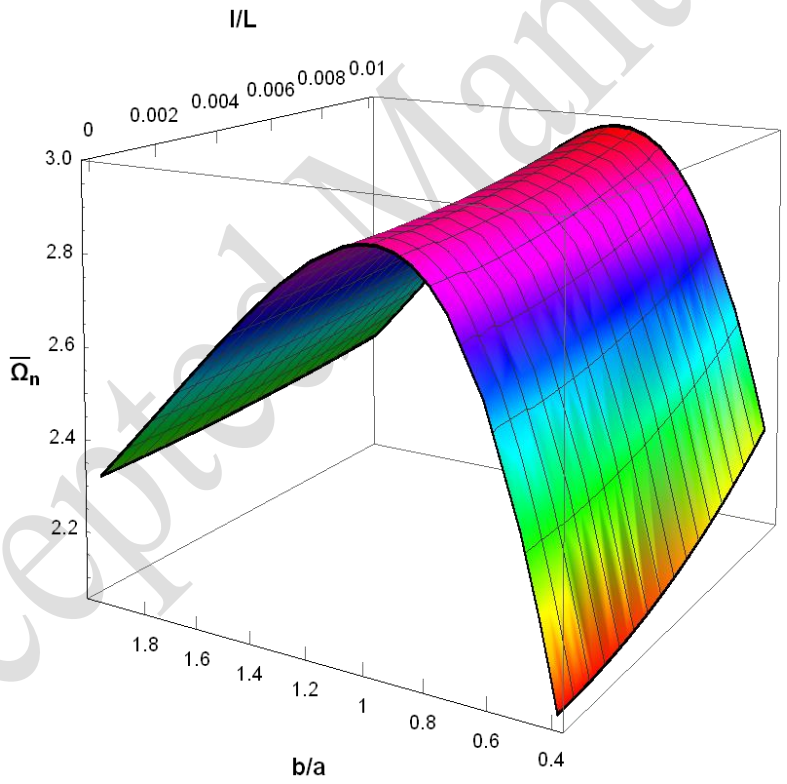

Fig. 7. Variation of the fundamental dimensionless natural frequency of the microrod model versus dimensionless material length scale parameter (l / L) and aspect ratio (b / a) under the clamped-clamped boundary condition ($a = 10$ μm and $L = 50$ μm).

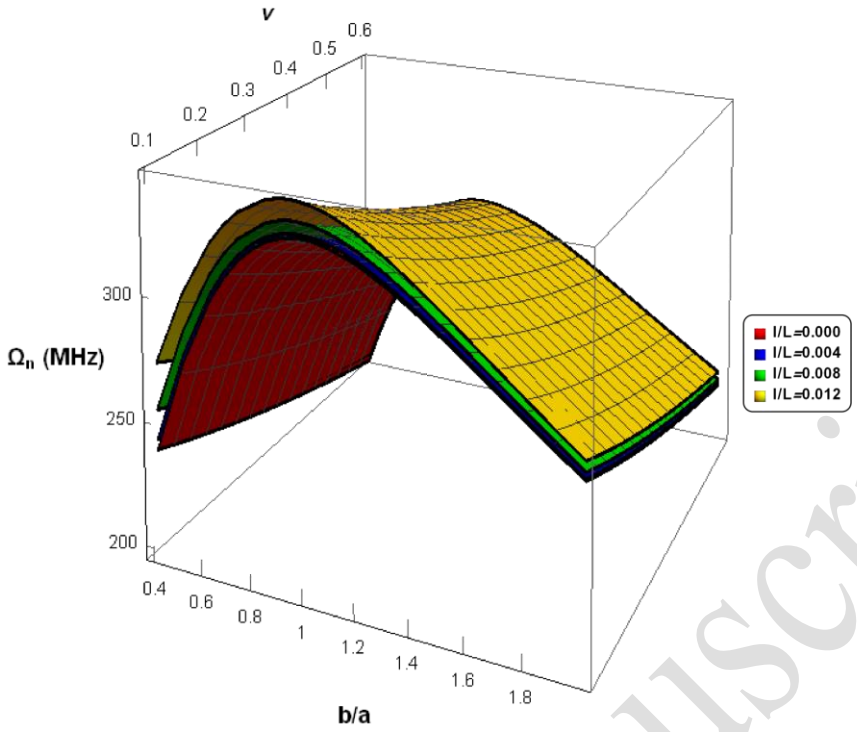

Fig. 8. Variation of the fundamental natural frequency of the microrod model versus aspect ratio (b/a) and Poisson's ratio for four various dimensionless material length scale parameters under the clamped-clamped boundary condition ($a = 10\ \mu m$ and $L = 50 \mu m$).

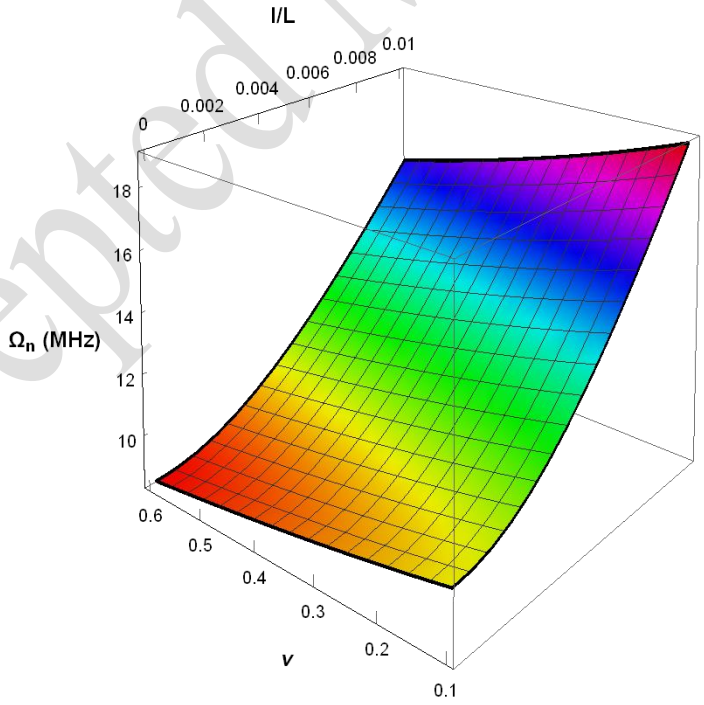

Fig. 9. Variation of the fundamental natural frequency of the microrod versus dimensionless material length scale parameter (l/L) and Poisson's ratio under the clamped-disk boundary condition ($b/a = 0.5, a = 10\ \mu m$, $L = 200\ \mu m$, and $I_d = 10^3 \mu^4 \times \left(N.m.s^2\right)$.

5. Conclusion

In this study, the size-dependent free torsional vibration of a microscale rod with a rectangular cross-section was investigated using the Modified Couple Stress Theory (MCST). The governing partial differential equation and the corresponding boundary conditions were derived through **Hamilton's principle** and subsequently reduced to an ordinary differential equation using the **Galerkin method**. To evaluate the influence of boundary conditions, the analysis was extended to include a **clamped-disk boundary condition** in addition to the fully clamped case. The key findings of this research are summarized as follows:

- The **dimensionless natural frequency** increases directly with both the **material length scale parameter** and the **mode number**. The minimum response occurs when the material length scale parameter is eliminated ($l / L = 0$) and only the fundamental frequency is considered.
- Increasing the material length scale parameter causes the **natural frequency** to decrease more sharply with respect to an increase in the **mass moment of inertia** of the attached disk, indicating a strong interaction between material microstructure effects and external mass.
- For **horizontal rectangles** ($a > b$), the natural frequency increases with increasing **aspect ratio** (b / a). Conversely, for **vertical rectangles** ($b > a$), the natural frequency decreases as the aspect ratio increases.
- Based on MCST, the **maximum natural frequency** occurs approximately at $b / a = 1$ for small material length scale parameters. However, as the material length scale parameter increases, the peak frequency shifts away from $b = a$, toward higher aspect ratios.
- The natural frequency of a **horizontal rectangle** is always greater than that of a **vertical rectangle**, given the same material and geometric properties.
- The presence of an **attached mass** increases the effective mass of the system, which in turn reduces the dimensionless natural frequency.
- For horizontal rectangles with lower values of the material length scale parameter, convergence of the solution occurs at **higher values of the series index** (i) in the shape function expansion.

These results highlight the importance of considering size effects through MCST to accurately simulate the dynamic behavior of microscale structures. These findings are useful for MEMS/NEMS device optimization and design, particularly where external attachments and torsional vibrations have a dominant role.

References

[1] B. Wiley, "Tiny glow sticks: Microrods made of lanthanoid organic frameworks act as microscale optical waveguides", *ScienceDaily*, 2017.

[2] J. Yang, C. Li, Z. Cheng, X. Zhang, Z. Quan, C. Zhang, J. Lin, "Size-tailored synthesis and luminescent properties of one-dimensional Gd2O3: Eu3+ nanorods and microrods", *The Journal of Physical Chemistry C*, Vol. 111, No. 49, pp. 18148-18154, 2007.

[3] H.-L. Yu, L. Li, X.-M. Gao, Y. Zhang, F. Meng, T.-S. Wang, G. Xiao, Y.-J. Chen, C.-L. Zhu, "Synthesis and H2S gas sensing properties of cage-like α-MoO3/ZnO composite", *Sensors and Actuators B: Chemical*, Vol. 171, pp. 679-685, 2012.

[4] M. Mandl, X. Wang, T. Schimpke, C. Kölper, M. Binder, J. Ledig, A. Waag, X. Kong, A. Trampert, F. Bertram, "Group III nitride core–shell nano-and microrods for optoelectronic applications", *physica status solidi (RRL)–Rapid Research Letters*, Vol. 7, No. 10, pp. 800-814, 2013.

[5] A. L. Campbell, S. D. Stoyanov, V. N. Paunov, "Fabrication of functional anisotropic food-grade micro-rods with micro-particle inclusions with potential application for enhanced stability of food foams", *Soft Matter*, Vol. 5, No. 5, pp. 1019-1023, 2009.

[6] H. Song, L. Zhang, F. Yu, B.-C. Ye, Y. Li, "Molecularly imprinted polymer functionalized nanoporous Au-Ag alloy microrod: Novel supportless electrochemical platform for ultrasensitive and selective sensing of metronidazole", *Electrochimica Acta*, Vol. 208, pp. 10-16, 2016.

[7] J. Medina-Valtierra, J. García-Servín, C. Frausto-Reyes, S. Calixto, "The photocatalytic application and regeneration of anatase thin films with embedded commercial TiO2 particles deposited on glass microrods", *Applied Surface Science*, Vol. 252, No. 10, pp. 3600-3608, 2006.

[8] G. Dai, Y. Zhang, R. Liu, Q. Wan, Q. Zhang, A. Pan, B. Zou, "Visible whispering-gallery modes in ZnO microwires with varied cross

sections", *Journal of Applied Physics,* Vol. 110, No. 3, pp. 033101, 2011.

[9] Z. Li, J. Zhang, J. Du, B. Han, J. Wang, "Preparation of silica microrods with nano-sized pores in ionic liquid microemulsions", *Colloids and Surfaces A: Physicochemical and Engineering Aspects,* Vol. 286, No. 1-3, pp. 117-120, 2006.

[10] R. Thirupathi, E. N. Prabhakaran, "Self-assembled microtubes and rhodamine 6G functionalized Raman-active gold microrods from 1-hydroxybenzotriazole", *Journal of Chemical Sciences,* Vol. 123, No. 3, pp. 247-254, 2011.

[11] A. Amarjargal, L. D. Tijing, H. R. Pant, C.-H. Park, C. S. Kim, "Simultaneous synthesis of TiO2 microrods in situ decorated with Ag nanoparticles and their bactericidal efficiency", *Current Applied Physics,* Vol. 12, No. 4, pp. 1106-1112, 2012.

[12] S. Narendar, S. Ravinder, S. Gopalakrishnan, "Strain gradient torsional vibration analysis of micro/nano rods", *International Journal of Nano Dimension,* Vol. 3, No. 1, pp. 1-17, 2012.

[13] S. Savel'ev, F. Nori, "Magnetic and mechanical buckling: Modified Landau theory approach to study phase transitions in micromagnetic disks and compressed rods", *Physical Review B,* Vol. 70, No. 21, pp. 214415, 2004.

[14] Y. Zhang, K. Han, X. Yin, Z. Fang, Z. Xu, W. Zhu, "Synthesis and characterization of single-crystalline PrCO3OH dodecahedral microrods and its thermal conversion to Pr6O11", *Journal of Crystal Growth,* Vol. 311, No. 15, pp. 3883-3888, 2009.

[15] L. Qi, Y. Xu, Z. Li, E. Zhao, S. Yang, B. Cao, J. Zhang, J. Wang, K. Xu, "Stress analysis of transferable crack-free gallium nitride microrods grown on graphene/SiC substrate", *Materials Letters,* Vol. 185, pp. 315-318, 2016.

[16] !!! INVALID CITATION !!! (Eringen 1983, Gurtin, Weissmüller et al. 1998, Aifantis 1999, Yang, Chong et al. 2002).

[17] M. Şimşek, "Nonlinear static and free vibration analysis of microbeams based on the nonlinear elastic foundation using modified couple stress theory and He's variational method", *Composite Structures,* Vol. 112, pp. 264-272, 2014.

[18] H. Salehipour, H. Nahvi, A. Shahidi, "Exact closed-form free vibration analysis for functionally graded micro/nano plates based on modified couple stress and three-dimensional elasticity theories", *Composite Structures,* Vol. 124, pp. 283-291, 2015.

[19] Z.-Y. Zhong, W.-M. Zhang, G. Meng, M.-Y. Wang, "Thermoelastic damping in the size-dependent microplate resonators based on modified couple stress theory", *Journal of Microelectromechanical Systems,* Vol. 24, No. 2, pp. 431-445, 2014.

[20] L.-L. Ke, Y.-S. Wang, "Flow-induced vibration and instability of embedded double-walled carbon nanotubes based on a modified couple stress theory", *Physica E: Low-dimensional Systems and Nanostructures,* Vol. 43, No. 5, pp. 1031-1039, 2011.

[21] M. Attia, F. Mahmoud, "Modeling and analysis of nanobeams based on nonlocal-couple stress elasticity and surface energy theories", *International Journal of Mechanical Sciences,* Vol. 105, pp. 126-134, 2016.

[22] L. Yin, Q. Qian, L. Wang, W. Xia, "Vibration analysis of microscale plates based on modified couple stress theory", *Acta Mechanica Solida Sinica,* Vol. 23, No. 5, pp. 386-393, 2010.

[23] R. Ansari, M. F. Shojaei, V. Mohammadi, R. Gholami, M. Darabi, "Nonlinear vibrations of functionally graded Mindlin microplates based on the modified couple stress theory", *Composite Structures,* Vol. 114, pp. 124-134, 2014.

[24] B. Akgöz, Ö. Civalek, "Free vibration analysis of axially functionally graded tapered Bernoulli–Euler microbeams based on the modified couple stress theory", *Composite Structures,* Vol. 98, pp. 314-322, 2013.

[25] B. A. Hamidi, S. A. Hosseini, R. Hassannejad, F. Khosravi, "An exact solution on gold microbeam with thermoelastic damping via generalized Green-Naghdi and modified couple stress theories", *Journal of Thermal Stresses,* pp. 1-18, 2019.

[26] C. Li, "Torsional vibration of carbon nanotubes: comparison of two nonlocal models and a semi-continuum model",

International Journal of Mechanical Sciences, Vol. 82, pp. 25-31, 2014.

[27] R. Ansari, R. Gholami, S. Ajori, "Torsional vibration analysis of carbon nanotubes based on the strain gradient theory and molecular dynamic simulations", *Journal of Vibration and Acoustics*, Vol. 135, No. 5, pp. 051016, 2013.

[28] X. Zhu, L. Li, "Longitudinal and torsional vibrations of size-dependent rods via nonlocal integral elasticity", *International Journal of Mechanical Sciences*, Vol. 133, pp. 639-650, 2017.

[29] S. Guo, Y. He, D. Liu, J. Lei, L. Shen, Z. Li, "Torsional vibration of carbon nanotube with axial velocity and velocity gradient effect", *International Journal of Mechanical Sciences*, Vol. 119, pp. 88-96, 2016.

[30] M. Hao, X. Guo, Q. Wang, "Small-scale effect on torsional buckling of multi-walled carbon nanotubes", *European Journal of Mechanics-A/Solids*, Vol. 29, No. 1, pp. 49-55, 2010.

[31] K.-C. Liu, J. Friend, L. Yeo, "The axial–torsional vibration of pretwisted beams", *Journal of Sound and Vibration*, Vol. 321, No. 1-2, pp. 115-136, 2009.

[32] G. Brabie, "The effects of torsion on the initial geometry of bars having non-circular cross-sections", *Journal of Materials Processing Technology*, Vol. 106, No. 1-3, pp. 8-12, 2000.

[33] A. Barr, "Torsional waves in uniform rods of non-circular section", *Journal of mechanical engineering science*, Vol. 4, No. 2, pp. 127-135, 1962.

[34] S. Christides, A. Barr, "Torsional vibration of cracked beams of non-circular cross-section", *International journal of mechanical sciences*, Vol. 28, No. 7, pp. 473-490, 1986.

[35] G. Yamada, T. Irie, Y. Tagawa, "Free vibration of non-circular cylindrical shells with variable circumferential profile", *Journal of Sound and Vibration*, Vol. 95, No. 1, pp. 117-126, 1984.

[36] F. Yang, A. Chong, D. C. C. Lam, P. Tong, "Couple stress based strain gradient theory for elasticity", *International Journal of Solids and Structures*, Vol. 39, No. 10, pp. 2731-2743, 2002.

[37] S. S. Rao, 2007, *Vibration of continuous systems*, Wiley Online Library,

[38] S. Christides, A. D. S. Barr, "Torsional vibration of cracked beams of non-circular cross-section", *International Journal of Mechanical Sciences*, Vol. 28, No. 7, pp. 473-490, 1986, https://doi.org/10.1016/0020-7403(86)90067-6.

[39] A. D. S. Barr, "Torsional Waves in Uniform Rods of non-Circular Section", *Journal of Mechanical Engineering Science*, Vol. 4, No. 2, pp. 127-135, 1962, 10.1243/jmes_jour_1962_004_019_02.

[40] A. Duwel, J. Gorman, M. Weinstein, J. Borenstein, P. Ward, "Experimental study of thermoelastic damping in MEMS gyros", *Sensors and Actuators A: Physical*, Vol. 103, No. 1-2, pp. 70-75, 2003.